# Design Analysis of the High-Speed Experimental Flight Test Vehicle HEXAFLY-International

Nunzia Favaloro[1], Attilio Rispoli[2], Ludovico Vecchione[3], Giuseppe Pezzella[4], Valerio Carandente[5], Roberto Scigliano[6], Marco Cicala[7], Gianfranco Morani[8]

*CIRA, Italian Aerospace Research Center, Via Maiorise, 81043 Capua (CE), Italy*

*and*

Johan Steelant[9]

*ESA-ESTEC, European Space Agency, Keplerlaan 1, 2200 AZ Noordwijk, The Netherlands*

**Achieving airbreathing hypersonic flight is an ongoing challenge with the potential to cut air travel time and provide cheaper access to space. Waveriders are potential candidates for achieving hypersonic cruise or acceleration flight within the atmosphere. Current research tends to focus on key issues like thermal loading, aero-elasticity and aerothermodynamics at hypersonic speeds. Design problems in each of these areas must be solved if a hypersonic waverider design is to be viable.**

**In this frame the HEXAFLY-INT project aims at the test in free-flight conditions of an innovative gliding vehicle with several breakthrough technologies on-board to be launched along a suborbital trajectory. Its preliminary conceptual design has been carried out by means of a number of numerical tools suitable to design vehicles flying in hypersonic conditions. The main results of the design analysis carried out during the preliminary phase of the study, such as vehicle aerodynamics and aerothermodynamics, re-entry trajectories, structures and mechanisms, and on the overall system, as well, are presented in this work.**

## Nomenclature

| | | |
|---|---|---|
| $AoA$ | = | angle of attack |
| $AoS$ | = | angle of sideslip |
| $b$ | = | wing span |
| $C_D$ | = | drag force coefficient |
| $C_L$ | = | lift force coefficient |
| $C_N$ | = | normal force coefficient |
| $C_Y$ | = | side force coefficient |
| $D$ | = | aerodynamic drag, diameter |

[1] Ph. D., Research Engineer, Aero-Space Technology Integration and Demonstrators Unit,, n.favaloro@cira.it

[2] Senior Research Engineer, Head of aeronautics flight lines &Demonstrators , Aero-Space Technology Integration and Demonstrators Unit, a.rispoli@cira.it

[3] Senior Research Engineer, Head of, Aero-Space Technology Integration and Demonstrators Unit,, l.vecchione@cira.it

[4] Ph. D., Research Engineer, Aerothermodynamic Section, Analysis and Extrapolation to Flight Lab., Head. g.pezzella@cira.it.

[5] Ph. D., Research Engineer, Thermo-structures and thermal control technologies and design Lab., v.carandente@cira.it

[6] Ph. D., Research Engineer, Thermo-structures and thermal control technologies and design Lab, r.scigliano@cira.it

[7] Ph. D., Research Engineer, Flight Mechanics Section , m.cicala@cira.it

[8] Ph. D., Research Engineer, Flight Mechanics Section , g.morani@cira.it

[9] Ph. D., Senior Research Engineer, ESA-ESTEC, Aerothermodynamics and Propulsion Analysis Section TEC-MPA, P.O. Box 299, Noordwijk, Netherlands, Johan.Steelant@esa.int, AIAA Member.

American Institute of Aeronautics and Astronautics

| | | |
|---|---|---|
| *E* | = | lift-to-drag ratio (aerodynamic efficiency) |
| *H, h* | = | altitude, height |
| *HF* | = | heat flux |
| *L* | = | length, aerodynamic lift, vehicle length |
| *L/D* | = | aerodynamic efficiency ($E_{ff}$) |
| *M* | = | Mach number, pitching moment, mass |
| *P* | = | pressure |
| *q* | = | heat flux |
| *S* | = | surface |
| *T* | = | temperature |
| *u, v, w* | = | velocity components |
| *V* | = | velocity, volume |
| *X,Y,Z* | = | coordinates |

*Greek Symbols*

| | | |
|---|---|---|
| $\alpha$ | = | angle of attack |
| $\beta$ | = | angle of sideslip |
| $\varDelta$ | = | variation |
| $\delta$ | = | aileron deflection |
| $\varepsilon$ | = | emissivity coefficient |
| $\gamma$ | = | specific heats ratio |
| $\rho$ | = | density |

# I. Introduction

Over the last years, innovative concepts of civil high-speed transportation vehicles were proposed. These vehicles have a strong potential to increase the cruise range efficiency at high Mach numbers, thanks to efficient propulsion units combined with high-lifting vehicle concepts. Performing a test flight at hypersonic speed will be the only and ultimate proof to demonstrate the technical feasibility of these new promising concepts versus their range efficiency.

CIRA, the Italian Aerospace Research Centre, in the framework of 7th Framework program with the European Space Agency and also thanks to international cooperation, is conducting a dedicated research project to develop the HEXAFLY-INT (High-Speed Experimental Fly Vehicles- INTernational) vehicle. This research program aims at the free flight testing of an innovative high-speed streamlined glider with several breakthrough technologies on board.

This approach will create the basis to gradually increase TRL. In order to mature the Hexafly-INT project, a scientific mission profile has been worked within a precursor, Level 0 project, called HEXAFLY followed by a proof-of-concept, based upon a preliminary design of a high-speed scramjet propelled flight test vehicle, the selection and integration of the ground-tested technologies developed within LAPCAT I & II, ATLLAS I & II and other national programs, and the identification of the most promising flight platform(s). About the last point, a waverider configuration has been selected to allow for a hypersonic cruise or acceleration flight within the atmosphere [1][2]

The present paper describes, after a general overview of the mission and vehicle requirements, at system and technologies levels, the main results of the design analysis carried out during the preliminary phase of the study, such as vehicle aerodynamics and aerothermodynamics, flight mechanics, structures and mechanisms, and on the overall system as well.

American Institute of Aeronautics and Astronautics

## II. Mission Objectives and Requirements

The HEXAFLY-INT project aims at the free flight testing of an innovative high-speed vehicle with several breakthrough technologies on board, the prime objectives of this free-flying high-speed cruise vehicle shall aim at:

- ➢ a conceptual design demonstrating a high aerodynamic efficiency at cruise with a high volumetric efficiency;
- ➢ a positive aerodynamic balance at a controlled cruise Mach numbers from 7 to 8;
- ➢ a good gliding performance from Mach 7 to 2;
- ➢ a maneuvering and control capabilities through the different flight regimes, guaranteed by a properly designed aeroshape and guidance and control system;
- ➢ an interface with a "service module for descent-not controlled phase" ;
- ➢ an optimal use of advanced high-temperature materials and/or structures.

The system architecture is such that HEXAFLY-INT project provides two main demonstrations:

- ✓ Mission level, aimed at validating the overall mission design and related operations aspects.
- ✓ System and sub-system level, aimed at validating vehicle design and sub-systems integration aspects.

## III. Mission Scenario

The HEXAFLY-INT design, manufacturing, assembly and verification will be the main driver and challenge in this project, in combination with a mission tuned sounding rocket (**Figure 1**).
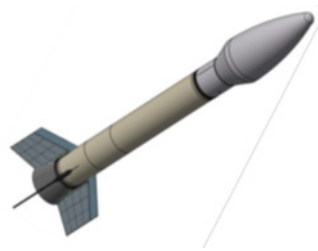


**Figure 1: HEXAFLY Launch Vehicle based on VS-43**

The Hypersonic vehicle will be launched in a suborbital trajectory, with the apogee at around 90 km altitude, by the VS43 Brazilian launcher; the choice of a guided rocket eliminated the concerns with respect to the a-symmetry of the payload and offered the potential of a hammerhead fairing.

After the release from launcher, the vehicle will be composed of two main parts, the Experimental Flight Test Vehicle (EFTV) and the Experiment Support Module (ESM). The former is the hypersonic glider that will perform the flight test; while the latter one (i.e., ESM) has the aim to control vehicle (i.e., EFTV+ESM) attitude by means of a cold gas system (CGS) when dynamic pressure does not allow controlling the EFTV by aerodynamic surfaces. The main preliminary flight sequence profile and events are shown and listed in Figure 2 and table 1 respectively.

American Institute of Aeronautics and Astronautics
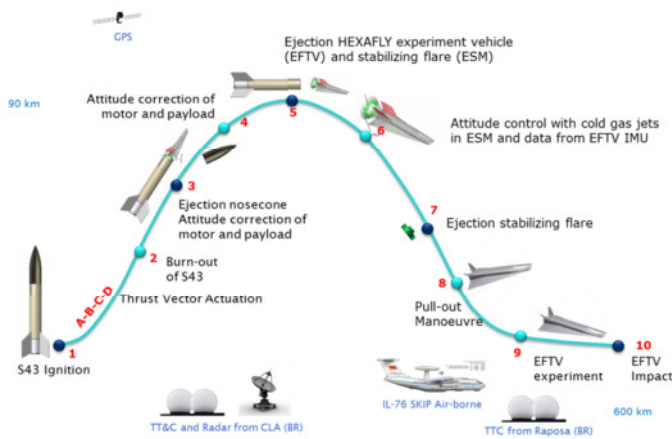
**Figure 2: Flight sequence profile**

**Table 1: Flight sequence Events**

| # | Flight Event |
|---|---|
| 1-2 | Propelled ascent |
| 2 | Motor burnout |
| 3 | Nose-cone ejection |
| 4 | L/V alignment |
| 5 | ESM/EFTV release |
| 6 | Attitude control by RCS in the ESM |
| 7 | Ejection of ESM |
| 8 | Pull-out maneuver |
| 9 | Controlled flight |
| 10 | Impact |

Only after the pull out maneuver the Experimental vehicle (i.e. EFTV) will execute an autonomous flight from hypersonic to subsonic regimes up to the splashdown, and the experimental flight will allow the demonstration of some objectives as high aerodynamic efficiency, a positive aerodynamic balance at controlled cruise Mach numbers, an optimal use of advanced high-temperature materials and structures.

## IV. System Conceptual Design Approach

The conceptual design approach here followed in order to design the Hexafly –INT configuration is characterized by the following steps:

  A.  Identification of vehicle configuration, and structures as a result of a trade-off among a set of candidate concepts in order to match the main objectives and requirements;
  B.  Definition of vehicle aerodynamics, able to guarantee the mission trajectory;
  C.  Definition of concept architecture in terms of  materials, on-board systems layout and other main subsystems

Here a summary of system and subsystems identification and details is given.

### A.  Vehicle Configuration and Structure

The overall aim of the HEXAFLY-INT project is to design, manufacture and test in flight a high speed gliding vehicle, based on the configuration developed in previously European community (EC) co-funded projects ATLLAS I & II, LAPCAT I & II, and HEXAFLY.[7] Under HEXAFLY-INT the scramjet propulsion system will not be developed further by the EC-partners, and as a consequence the flight experiment is focused on a self-controlled glider configuration.

The EFTV vehicle configuration is reported in Figure 3, where the train (i.e. EFTV docked to ESM) and ESM configurations are provided as well.
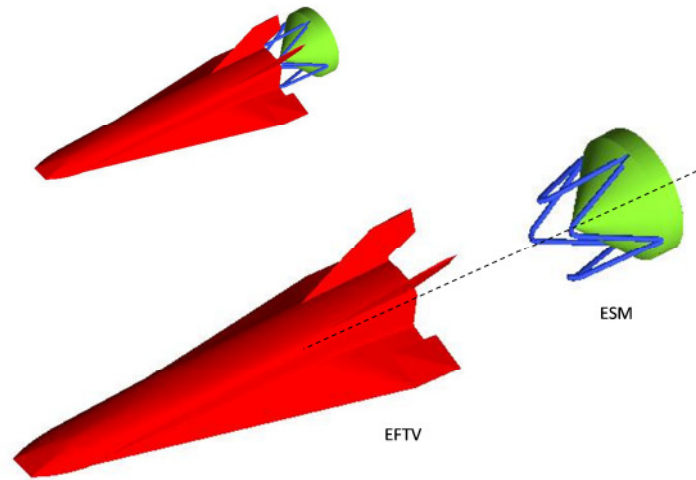
**Figure 3: EFTV docked to ESM, EFTV and ESM aeroshapes.**

The vehicle design makes maximum use of databases, expertise, technologies and materials elaborated in previously European community  co-funded projects ATLLAS I & II, LAPCAT I & II, and HEXAFLY.[7]

As stated before, the evolution of the EFTV glider configuration has started by the HEXAFLY propelled vehicle, namely the V47 aeroshape.  The intake and the nozzle of the scramjet propulsion flow path were closed. A simple flat panel closed the nozzle as a classical base, while a cap, namely Cap_V7, was conceived to close the scramjet inlet of the V47 aeroshape. This cap was constructed in such a way that the upper surface downstream of the leading edge was connected tangentially to the original inlet. Upstream of this panel and the original leading edge, a conical nose was attached. The upper panel of the cone had in the symmetry plane an angle of 7 deg while the lower inclination was 16 deg.

**Figure 4**, shows different views of the HEXAFLY-INT EFTV with the Cap_V7 (in green). In this way, the aeroshape Cap_V7 was obtained and delivered by DLR. Such a Cap_V7 configuration guaranteed an aeroshape which featured, in clean configuration, a natural trim point if the moment reference centre was considered at 57% of $L_{ref}$.
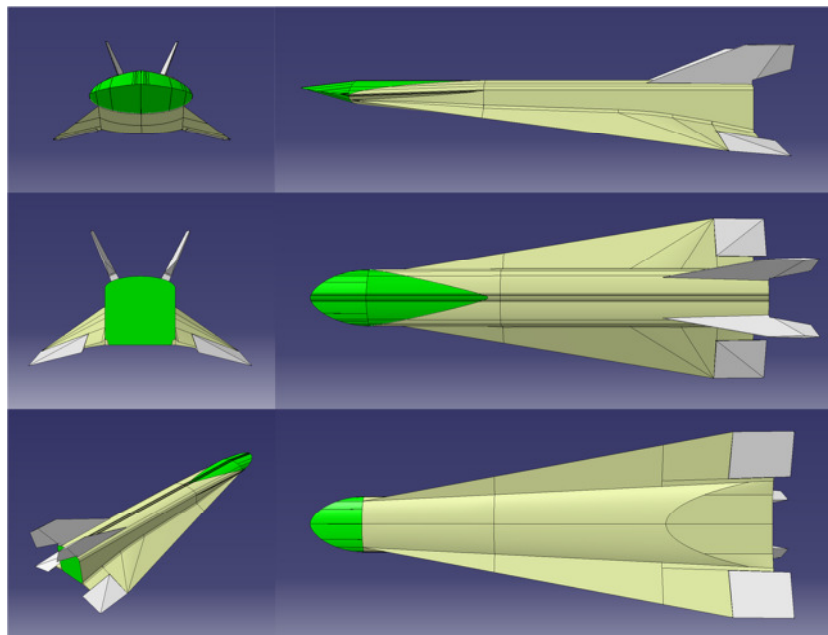


**Figure 4: EFTV Cap_V7 aeroshape by DLR.**

American Institute of Aeronautics and Astronautics

Starting from this aeroshape further changes have been operated, on the basis of suggestions coming from preliminary CFD analyses. The leading edge of the cap was modified, moving from a 3-D to a 2-D leading edge, as shown in Figure 5. This change simplified leading edge manufacturing and was characterized by lower aero-heating with respect to the Cap_V7. In this way, the aeroshape C4 was obtained by CIRA.
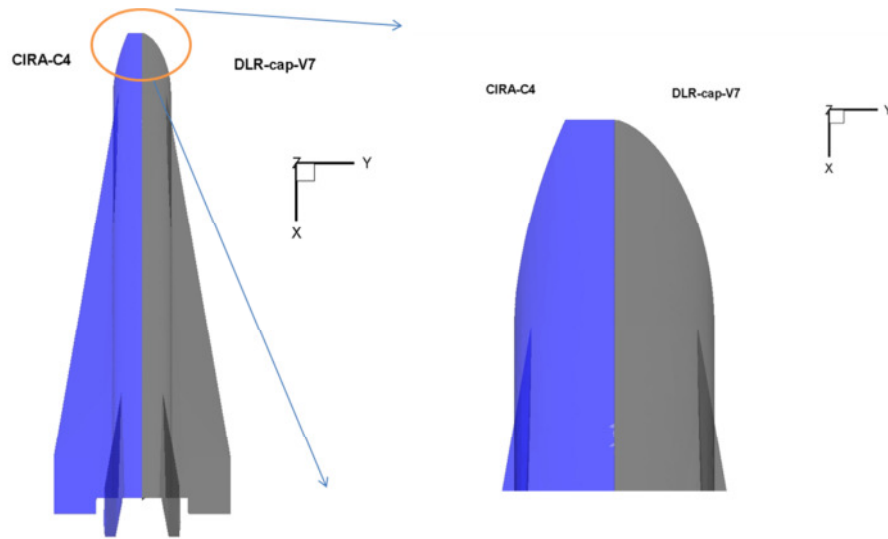


**Figure 5: EFTV forebody. Comparison between DLR-Cap_V7 and CIRA-C4 aeroshapes.**

The comparison between DLR-Cap_V7 and CIRA-C4 aeroshapes in terms of lift-to-drag ratio (L/D) and pitching moment coefficient is shown in Figure 6. As one can see, this aeroshape update has not affected significantly the vehicle's aerodynamic performance.
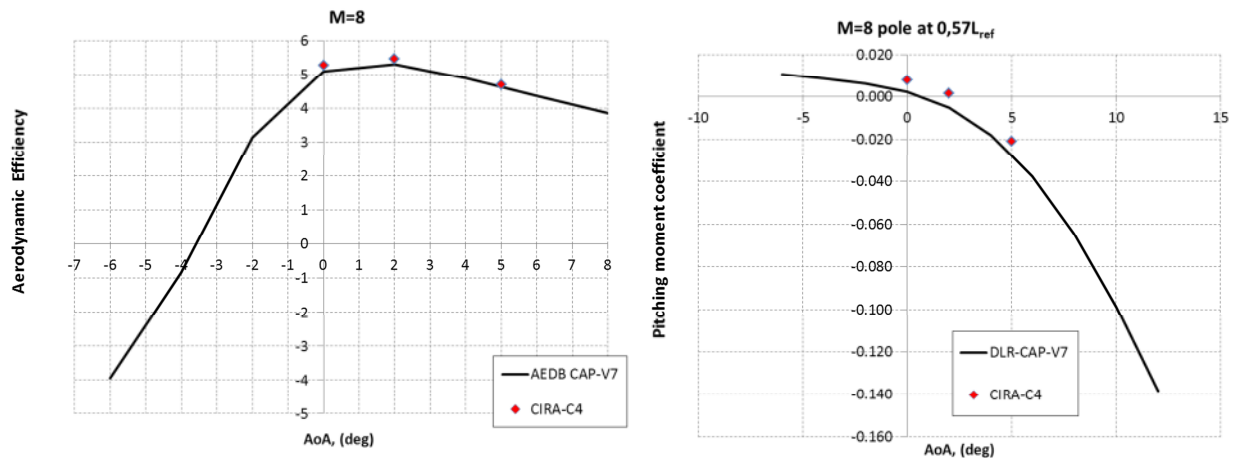


**Figure 6: Comparison between DLR-Cap_7 and CIRA-C4 in terms of L/D and Cm.**

However, pressure and heat flux surface distributions on the Cap_V7 forebody leeside feature non-smooth fields, as summarized in Figure 7.

American Institute of Aeronautics and Astronautics
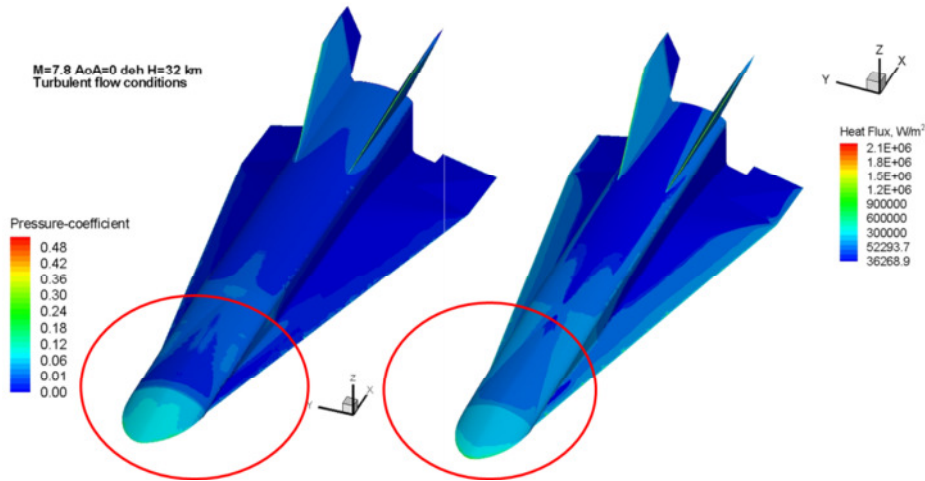
**Figure 7: Pressure and heat flux surface distributions for the DLR-Cap_7 aeroshape.**

This fact has suggested improving locally the vehicle's aeroshape. Above results encouraged CIRA to verify margin improvements on the Cap_V7 forebody leeside. To this end the CIRA-FC4 forebody has been proposed and investigated. Aeroshape modification moving from CIRA-C4 aeroshape to CIRA-FC4 aeroshape is shown in Figure 8



HEXI-CIRA-C4                    HEXI-CIRA-FC4
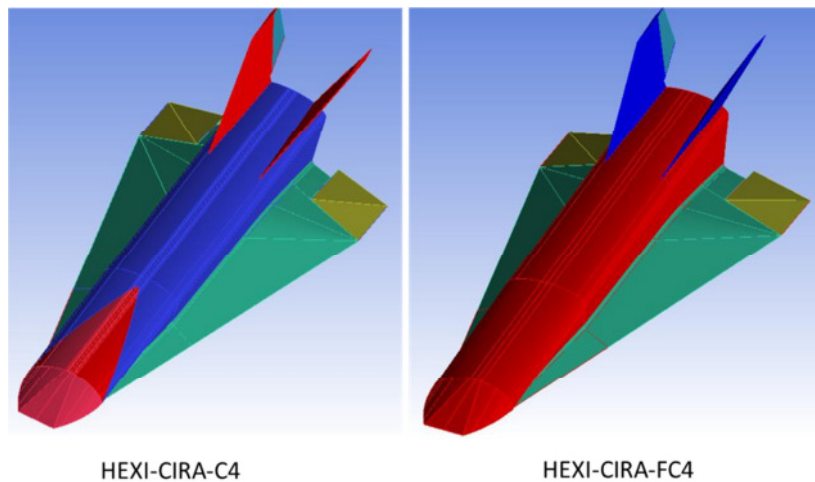
**Figure 8: Comparison between CIRA-C4 and CIRA-FC4 aeroshapes.**

Surface improvements operated on the CIRA-FC4 aeroshape can be appreciated on the comparison of pressure distribution reported in Figure 9, evaluated for M∞=8 and AoA=0 deg freestream conditions. This surface change does not affect vehicle aerodynamic performance provided that L/D and pitching moment coefficients for the CIRA-FC4 confirm the results shown in Figure 6.
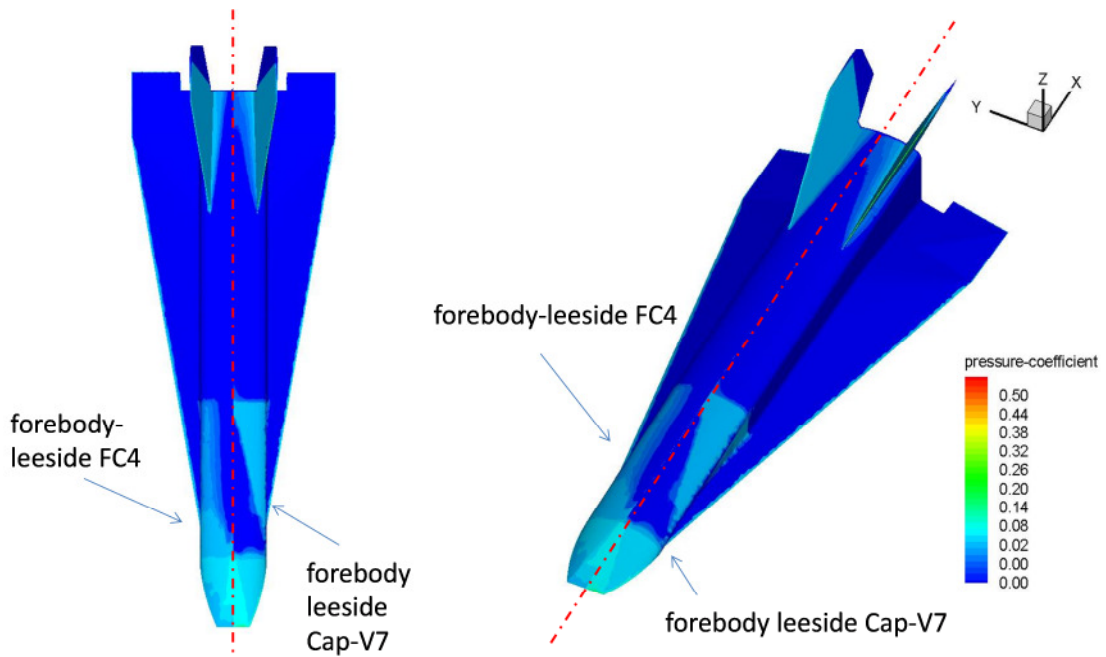
**Figure 9: Pressure distribution comparison between CIRA-C4 and CIRA-FC4.**

However, also in the FC4 configuration there were bulges and indents which made the manufacturing and assembly more difficult and costly. So, in order to simply the vehicle manufacturing and to allow structural feasibility (the aeroshape features a very slender configuration) of the vehicle in the light of external loading conditions and internal subsystem layout, i.e. avionics, aerodynamic surface actuators and etc., vehicle aeroshape was further modified into the current configuration, namely CIRA-FC4RF. This last aeroshape with main modification is shown in Figure 10 and Figure 11. On the left of Figure 10, bottom is reported the cross section at x=114.727 mm, while on the right the one at x=573.636 mm. Here the white line refers to the FC4RF aeroshape section, while in red is reported the FC4 aeroshape section.

American Institute of Aeronautics and Astronautics
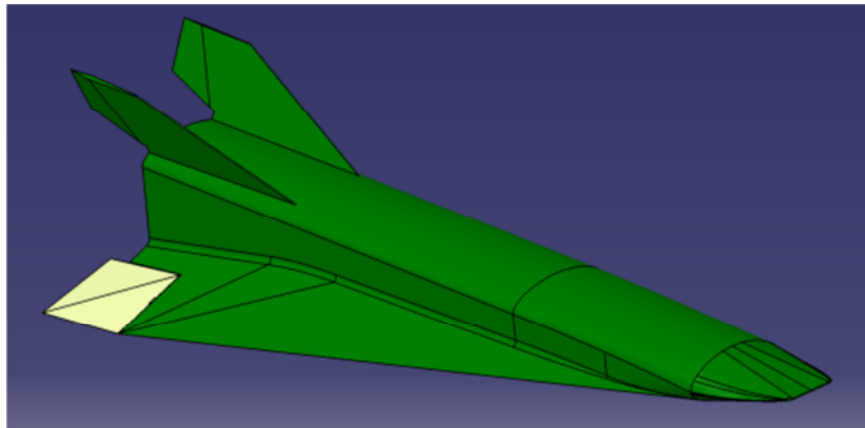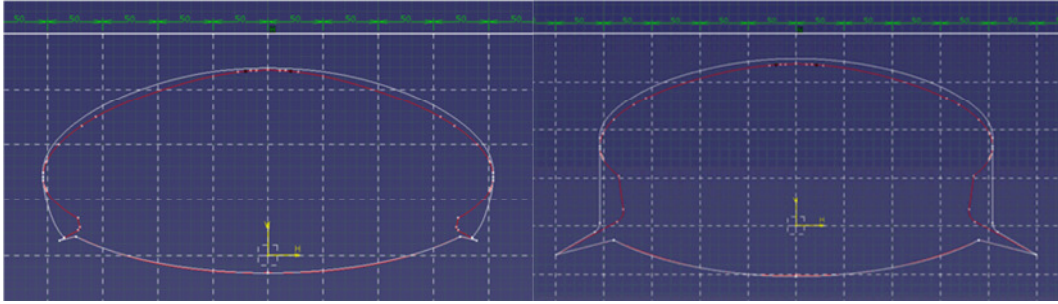
**Figure 10: CIRA-FC4RF complete aeroshape (top) and comparison of cross sections (bottom, in white) with CIRA-FC4 aeroshape (in red).**

In the meantime thermal analysis and the requirement to realize the vehicle nose with metallic material pointed out the need to consider a fillet at least of 2 mm at nose leading edge with rounding at corners, as shown in Figure 11. In this way one is able to alleviate local hot spots on the left and right ends of the 2D nose leading edge and the previous sharp edges were laterally rounded off (see also Figure 8).



Lateral rounding at the nose leading edge to avoid local over-heating

2mm nose leading edge radius
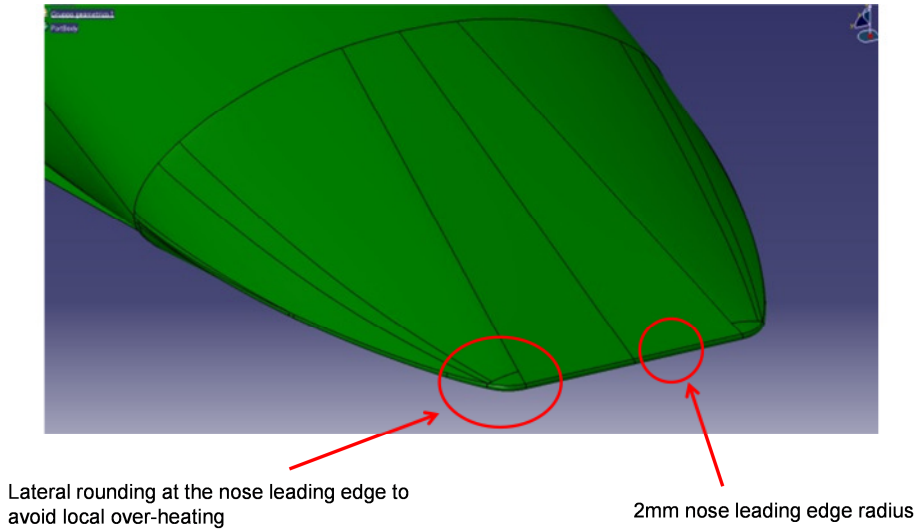
**Figure 11: CIRA-FC4RF details of the forebody leading edge.**

Aerodynamic performances comparison at $M_\infty=8$ between CIRA-FC4 and CIRA-FC4RF is summarized Figure 12. As one can see, CIRA-FC4RF performances at $M_\infty=8$ do not significantly change, but a CoG shift from 0.57 $L_{ref}$ to 0.579 $L_{ref}$ is needed to get natural trim conditions in clean configuration (see Figure 12).



9

American Institute of Aeronautics and Astronautics
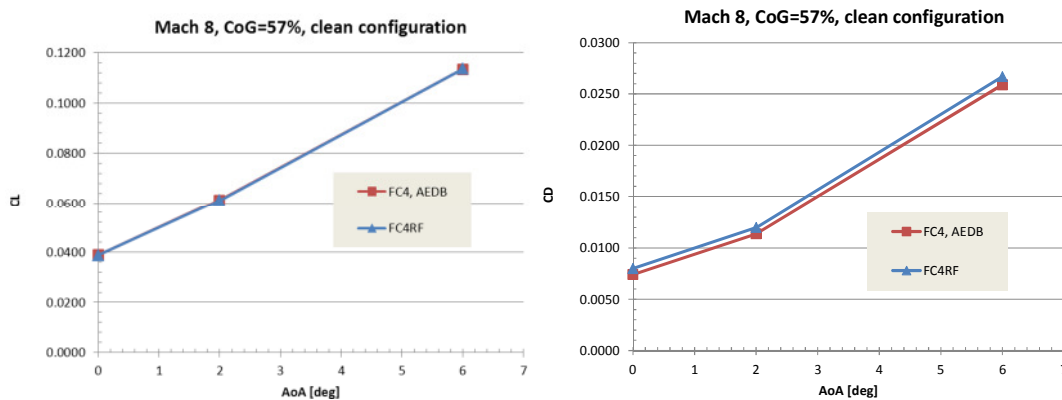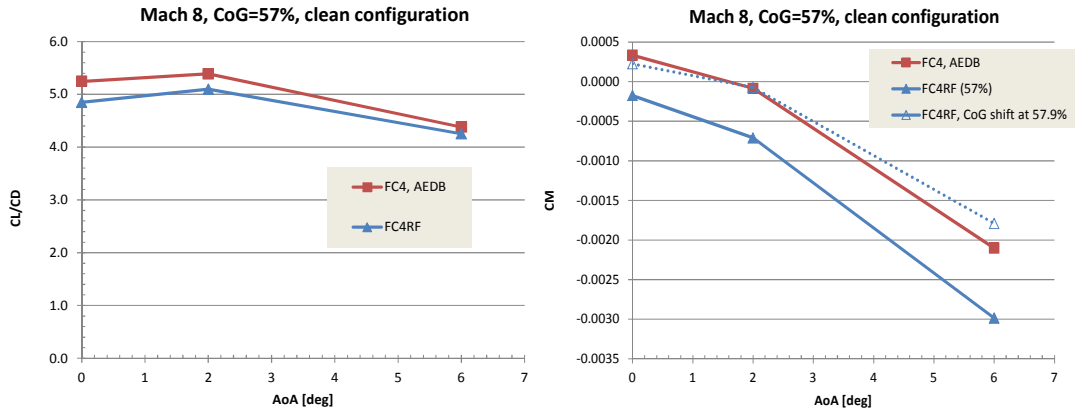
**Figure 12: Aerodynamic performance comparison at M=8 between CIRA-FC4 and CIRA-FC4RF.**

The latest nose cap modification shows that there is no loss in aerodynamic performance, thus encouraging to continue in the vehicle design activities.

At this stage, the Hexafly-INTernational vehicle is long 4 m and has a max wing span of 1.24 m. The EFTV configuration under consideration is depicted in Figure 13.

The Experimental Vehicle is characterized by relatively simple architecture, which embodies all the features of an operational system. The concept consists of a truncated waverider wing with vertical stabilizers and a fuselage on top of the wing.
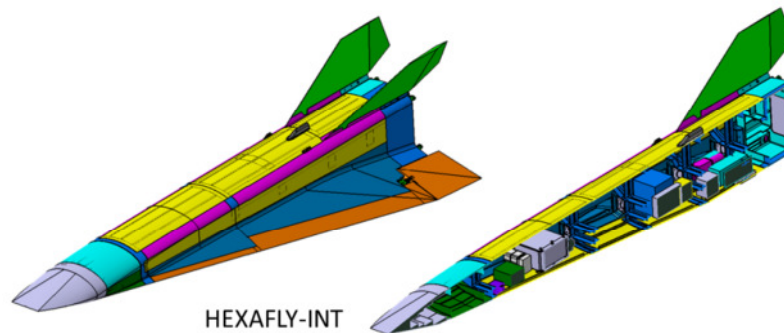


**Figure 13: Hexafly-International layout**

The internal layout has been designed to allocate the cargo bay and relevant equipment in the limited volume, and with a limited maximum weight allowable by the launcher. The system relies, at the maximum extent, on flight proven or on-ground qualified sub-systems and equipment developed within international projects. Further, the use of COTS H/W coming from space and aeronautics heritage is strongly recommended.

The HEXI configuration is made of two main structure, Cold structures and Hot structure, herein briefly described. The cold structure of EFTV is composed mainly by the whole experimental vehicle except the following item: Ailerons, Leading edge and Nose cap. For the experimental flight vehicle, several substructures can be identified, as shown below (Figure 12):

- ✓ fuselage structure
- ✓ rudders
- ✓ wings

American Institute of Aeronautics and Astronautics
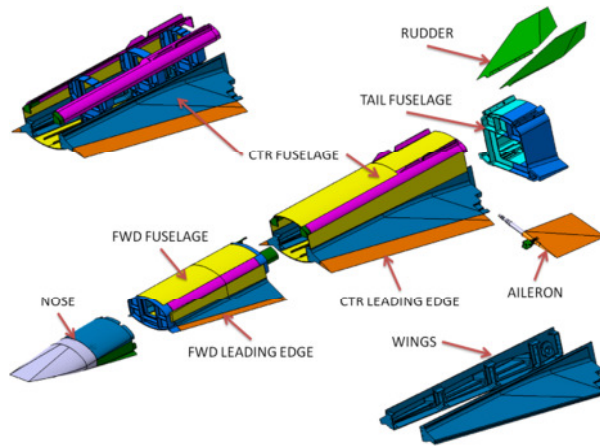
**Figure 14: EFTV main components**

The hot structures of EFTV are composed mainly by the following subsystems: Ailerons, Leading edge and Nose cap that is composed by three parts one fully solid body, the other are two shell upper shell and lower shell longitudinally joint.
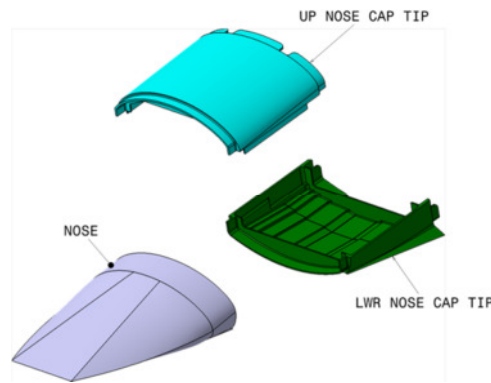


**Figure 15: Nose Cap exploded view**

A particular attention, during the design phase, was made to the mass property and performance.
The weight for the whole mission has been estimated below 450 kg with a margin and within the launcher limit and any mass growth shall be avoided because it induces increase in nominal speed with increasing demand for control system

The centre of gravity is located at 75% of fuselage length, and the equipment's allocation inside the vehicle is very critical considering the very limited internal volume implying detailed thermal control analysis and integration issues that will be covered in the next phase of the study.
In order to highlight the different contribute related to EFTV system, in the following table, the system is divided in three different areas:

- Structure
- Telemetry
- Flight Control

American Institute of Aeronautics and Astronautics

| Sub System | Mass [kg] |
|---|---|
| EFTV Structure | 318 |
| EFTV Telemetry | 11 |
| EFTV Flight Control | 32 |
| **EFTV Weigh** | **362** |
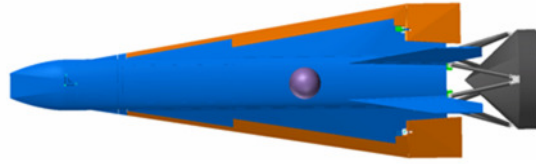


**Figure 16:  EFTV mass breakdown**

## B.  Aerodynamics characteristics

The aerodynamic data of EFTV presented in this paper are results of inviscid CFD computations performed by DLR and Navier-Stokes simulations (both laminar and turbulent) carried out by CIRA. This overview refers to EFTV aeroshape called FC4, i.e. the one used by DLR to build-up the full AEDB, according to the Table 2

| δ [°] | M [-] | α [°] | β [°] |
|---|---|---|---|
| -20 to +5  with Δδ =5 | 2 to 9 with ΔM=1 | -6 to +12 with Δα=2 | 0 and 2 |

**Table 2. Matrix of flow conditions and flap defections for the EFTV aerodynamic database.**

In the following a few selected plots of aerodynamic data are shown. For instance, Figure 17 provides an overview of the lift and drag coefficients as a function of Mach number with and without sideslip angle and aileron deflections effects. As shown, 2 deg sideslip angle does not change vehicle lift force, but negative aileron deflections (-5 and -10 in figure) significantly reduce the lift coefficient. For what concerns drag, Figure 17 points out that neither sideslip angle of 2 deg nor flap deflections of -5 and -10 deg determine considerable variation in drag. However, it is worth to note that these results refer to inviscid flowfield evaluations, i.e. the detrimental effect on aerodynamic performance of eventual local flow separations are not still accounted for.
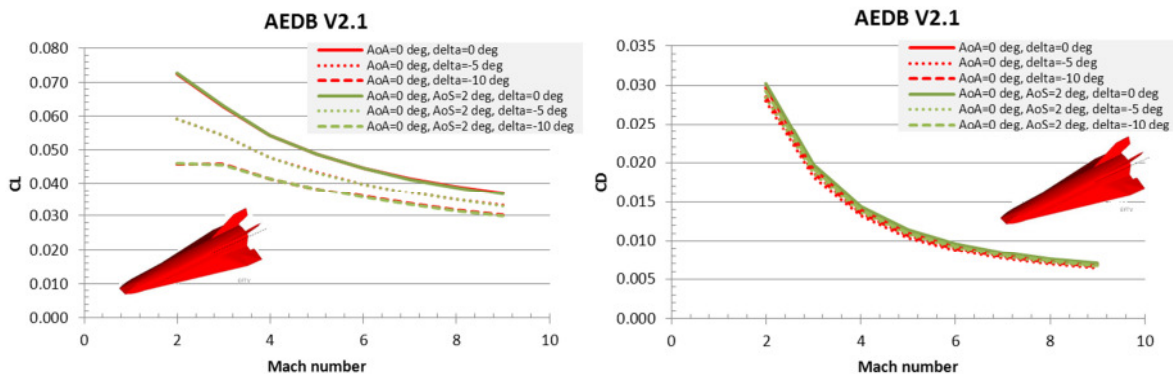


**Figure 17: $C_L$ and $C_D$ vs. Mach number with and without sideslip angle and aileron deflection effects.**

The same evaluation but for lift-to-drag ratio and pitching moment coefficient is summarized in Figure 18.

American Institute of Aeronautics and Astronautics
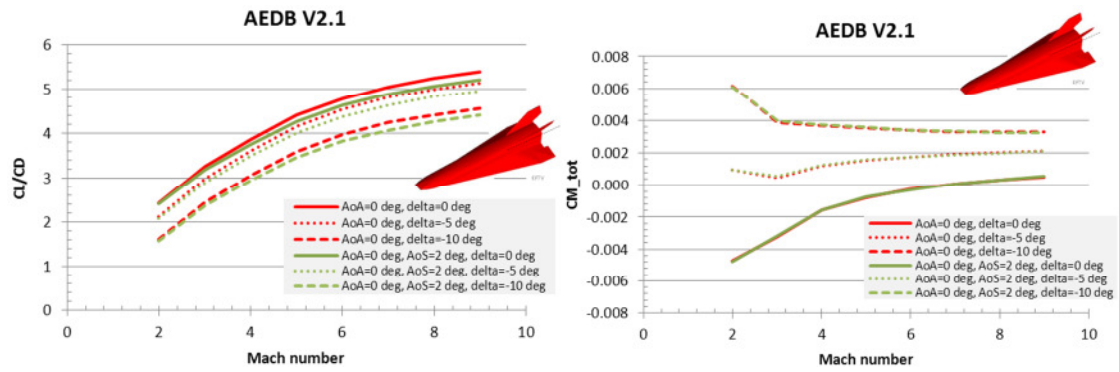
Figure 18: L/D and $C_m$ vs. Mach number with and without sideslip angle and aileron deflection effects.

As one can see, the lift-to-drag ratio evolves accordingly to above suggestions for lift and drag, as shown in Figure 18. On the other hand, the pitching moment coefficient suggests that again 2 deg of sideslip flow does not markedly change $C_m$, but aileron deflections move upward the pitching moment characteristic, as expected. Note that in the Mach number range from 7 to 8, and AoA=0 deg, some conditions of natural trim (delta=0 deg) or trim obtained with a small positive aileron deflection (lower than 1 deg) are predicted.

The effect of aileron deflection on aerodynamic efficiency L/D at different angles of attack and at $M_\infty$=2, 4, 6 and 8 is summarized in Figure 19.
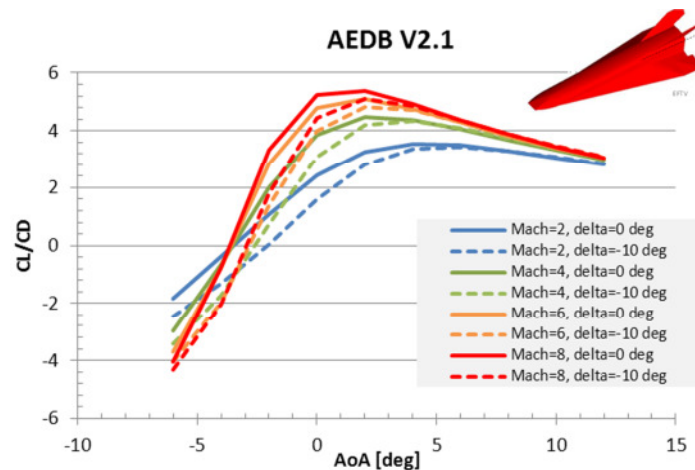


Figure 19: L/D vs. AoA at M=2, 4, 6, 8 and for 0 deg and -10 deg aileron deflections.

As shown, the aerodynamic efficiency is greater than 4 for Mach=6÷8 and AoA=-1÷7 deg. Anyway, some degradation of aerodynamic efficiency is expected when considering viscous effect evaluations.

The evolution of the pitching moment coefficient versus angle of attack for different Mach numbers (i.e. 2 and 8) and aileron deflections (i.e. 0, -5, -10, -15, and -20 deg) is summarized in Figure 20 .[7] For instance, Figure 21 points out that at $M_\infty$=2 the EFTV aeroshape FC4 can be trimmed with proper aileron deflections from about -4 to 10 deg angle of attack.

American Institute of Aeronautics and Astronautics
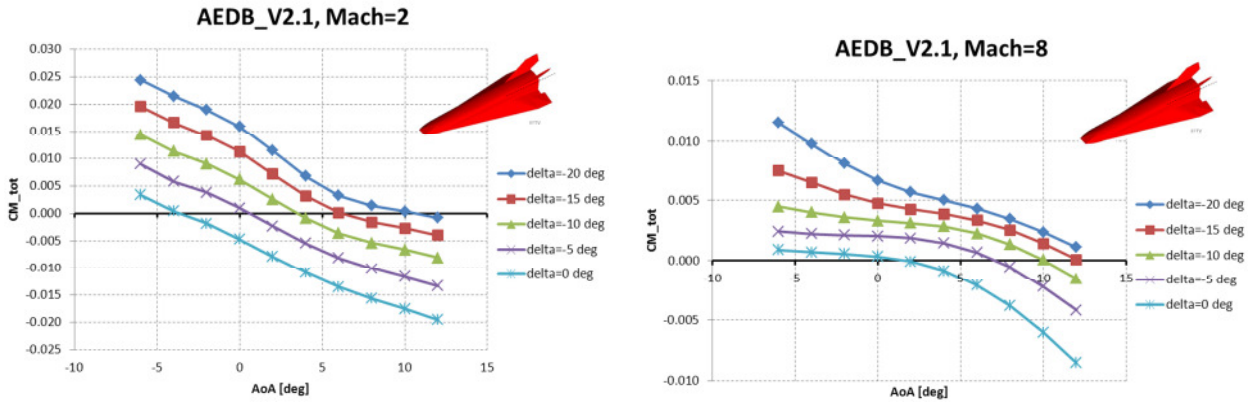
**Figure 20: Pitching moment coefficient versus AoA at different aileron settings at $M_\infty$=2, 4, 6, and 8.**

At $M_\infty$=8 these ranges are (-1, 12) deg and (2, 12) deg, respectively. Moreover, no significant effects of sideslip, for both clean and trimmed configurations are foreseen, as summarized in Figure 20.
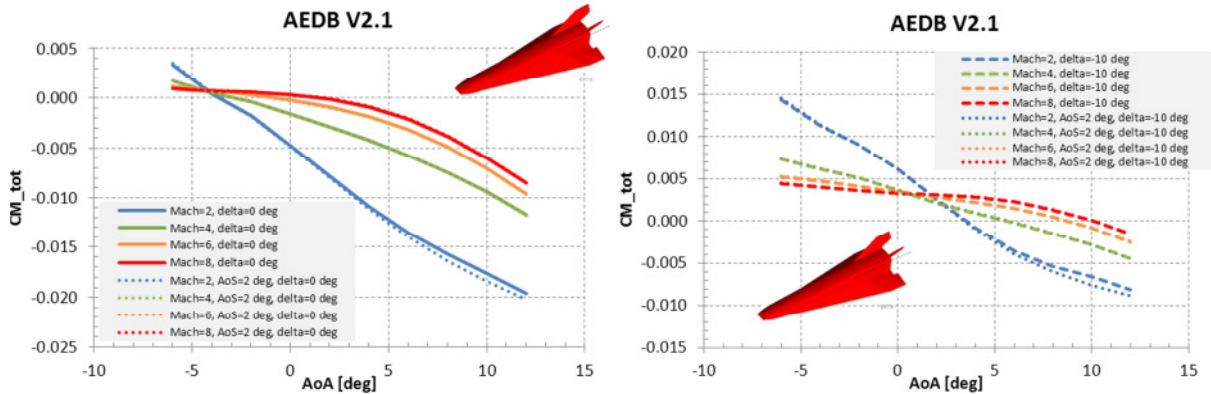


**Figure 21: $C_m$ versus AoA at different Mach numbers and with and without sideslip angle effects.**

As far as static stability in longitudinal and lateral-directional flight conditions is concerned, Figure 21 indicate that the glider is statically stable in longitudinal flight conditions.

On the other hand, the derivatives with respect to sideslip angle of side force, rolling moment and yawing moment coefficients at different Mach numbers and angles of attacks are summarized from Figure 22 to Figure 24. As one can see, also in lateral directional flight conditions the vehicle features static stability. In particular, Figure 22 points out that speed disturbance stability (i.e. $C_{Y_\beta}$<0) is predicted at all Mach numbers and AoAs here investigated.
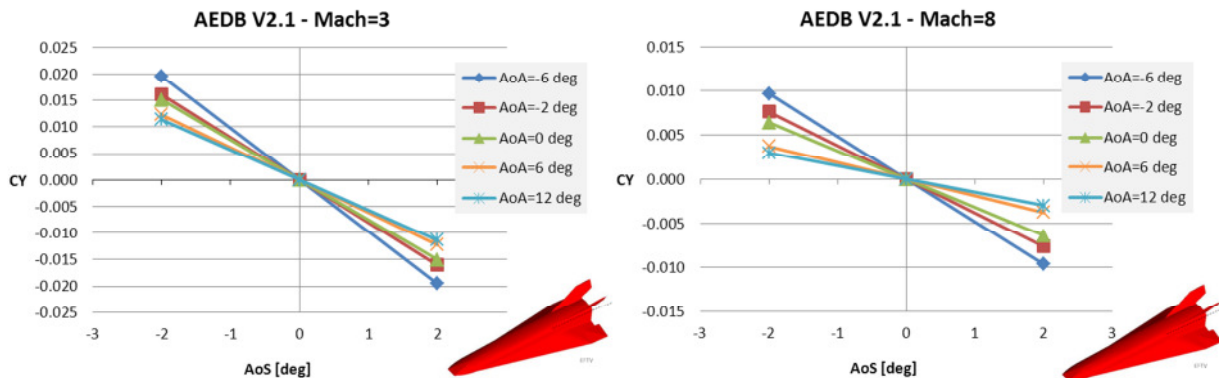


**Figure 22: $C_Y$ versus AoS at different AoA at $M_\infty$=3 and 8.**

14

American Institute of Aeronautics and Astronautics

The sideslip derivative of the rolling moment coefficient $C_l$ is provided in Figure 23 at five angles of attack, namely -6, -2, 0, 6, and 12 deg. As one can see, dihedral effect stability is predicted at all Mach numbers for AoA ≥ 0 deg.
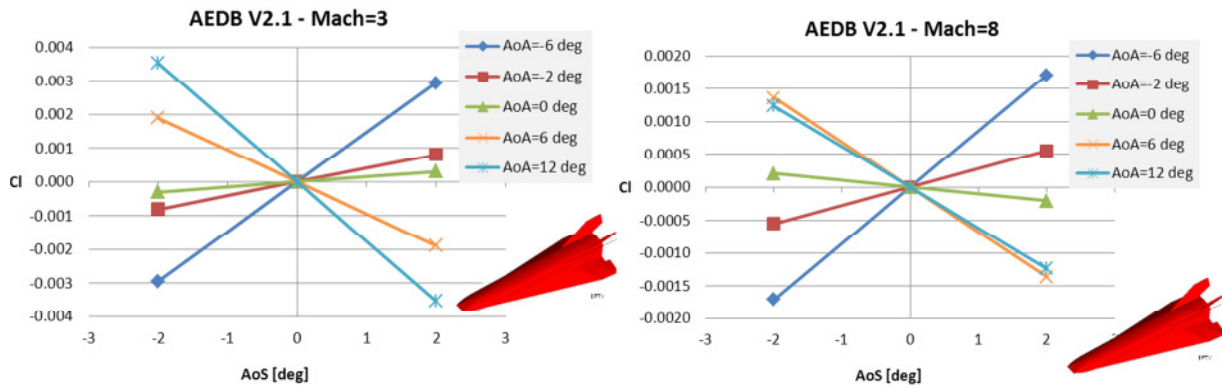


**Figure 23: $C_l$ versus AoS at different AoA at $M_\infty$=3 and 8.**

Finally, the sideslip derivative of the yawing moment coefficient $C_n$ is provided in Figure 24, at five angles of attack, namely -6, -2, 0, 6, and 12 deg. As shown, the weathercock lateral stability is predicted at all Mach numbers and AoAs.
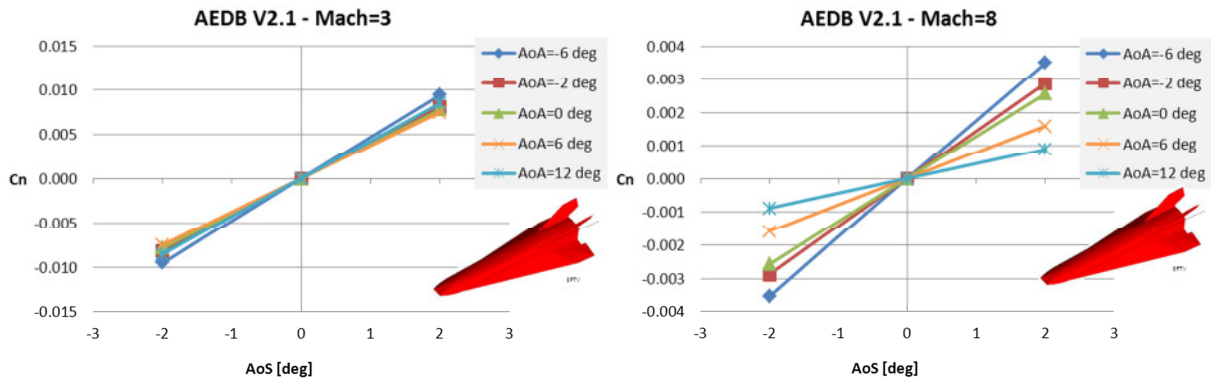


**Figure 24: $C_n$ versus AoS at different AoA at $M_\infty$=3 and 8.**

## C. Concept architecture and subsystem

### *Aeroheating and Materials*

Once the trajectories are provided, the aero heating environment that the vehicle concept has to withstand along its lifting re-entry flight has to be determined. During the flight, in fact, the vehicle suddenly heats due to the dissipation in the boundary layer of its high internal energy (potential and kinetic) by friction with the atmosphere. Vehicle surface heating strongly depends on the re-entry vehicle aero shape and attitude. Moreover, a material trade-off has been performed leading to take into account different material for the EFTV structure, namely: titanium alloy, copper, C/C-SiC and zirconia for surface coatings. Titanium alloys exhibit a unique combination of mechanical and physical properties and corrosion resistance which have made them desirable for critical, demanding aerospace applications, also in high temperatures conditions. Copper is employed as a heat sink to accommodate the thermal energy in some critical

American Institute of Aeronautics and Astronautics

components (e.g. nose, leading edges)[4]. C/C-SiC developed at DLR and tested in different high temperatures applications (e.g. HIFiRE and SHEFEX) is considered for ailerons and for almost the totality of the wing leading edge[6]. A zirconia coating layer has been also considered to protect titanium and copper components, increasing the surface emissivity and confining the larger temperatures on the layer itself.

Finally, the following assumptions, summarized in Table 3, have been carried out on the vehicle components shown in Figure 25 [8,9]:

- copper for the vehicle nose;
- copper for the fore part of the wing leading edges;
- C/C-SiC for the remaining part of the wing leading edge;
- copper for the leading edge of the tails;
- C/C-SiC for the ailerons;
- titanium alloy for the remaining part of the structure.

In addition, a layer of 1 mm thick zirconia has been foreseen for all the components in titanium alloy and copper. Using a conservative approach, a constant surface emissivity of 0.4 has been set for the external coated surfaces.
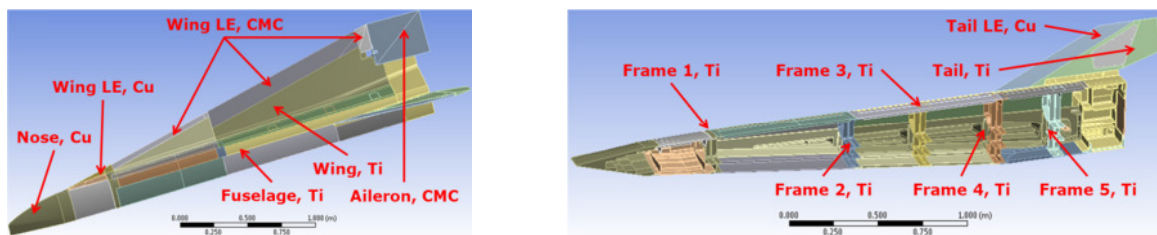


**Figure 25: Main structural components of the analysed EFTV**

**Table 3: Preliminarily material assignment for the main structural components**

| Nose | Fuselage | Wing | Wing LE | V-Tail | Aileron |
|---|---|---|---|---|---|
| Copper | Ti-Alloy | Ti-Alloy | C/C-SiC / Copper | Ti-Alloy / Copper | C/C-SiC |

The vehicle thermal behaviour has been preliminary assessed by means of the Finite Element Method (FEM) implemented in the software Ansys. A transient analysis along the computed entry path is performed to evaluate the time dependent temperature of the structure.

As results, the temporal variation of the maximum temperature on the different analysed materials and vehicle components has been plotted along the flight path. Figure 26 reports in particular the maximum temperature variation along the flight profile on the main vehicle components.

From Figure 26 it can be seen that zirconia coatings and C/C-SiC components (having maximum service temperatures in the order of 2400°C and 1600°C, respectively) would widely survive the aerothermal environment in these conditions. On the other hand, it can be noted that the maximum temperatures on the titanium and copper structures slightly exceed their upper working temperature limits (600 and 800°C, respectively), but only in limited spots of the vehicle, coloured in red for the titanium structure in Figure 27. This means that such temperature overshoot can be in principle redistributed inside the vehicle structure through a future thermal structural optimization.
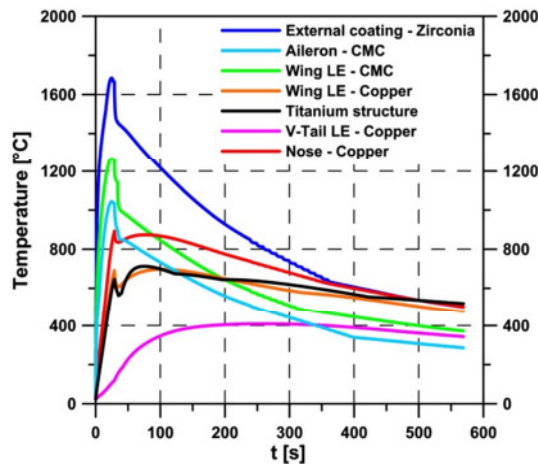
**Figure 26: Maximum temperature along the flight profile on the main vehicle components**
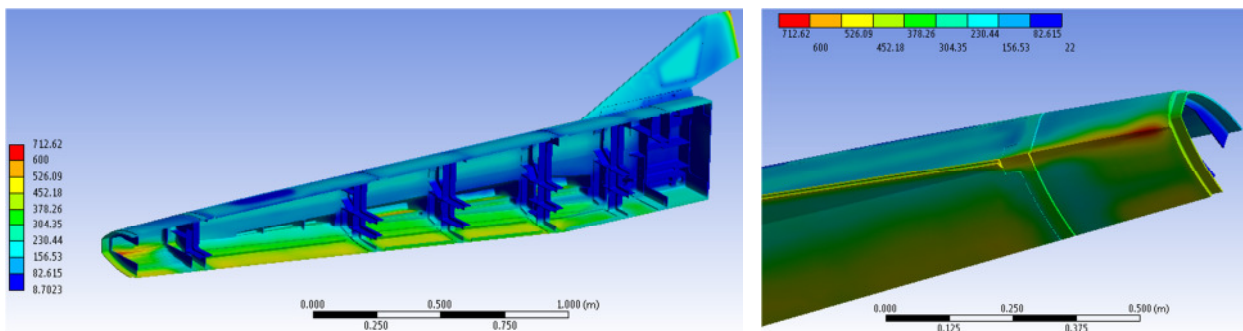


**Figure 27: Temperature distribution on the titanium structure at the peak heating condition for titanium components**

Finally, from a thermal structural point of view, it can be concluded that:
- a thermal model has been realized for the entire structure on the basis of aerothermal loads estimated along the flight path;
- zirconia coating guarantees a relatively large surface emissivity and a suitable thermal protection for the underlying materials;
- copper seems to be adequate for the nose and the first part of the wing leading edge, considering its ability to work as a heat sink;
- copper and titanium structures can withstand the aerothermal environment except for limited spots, requiring a proper thermal structural optimization;
- thermal structural design is still ongoing and a numerical analysis campaign will be performed on updated structural configuration.

## On Board Systems

The Hexafly-International vehicle employs an avionic system comprised of an inertial measurement unit (IMU), GPS, control actuators, and a flight control computer. Other subsystems include batteries for electrical power, servo control boards, power switching boards, sensors to measure pressure and temperature on the outside and inside of the vehicle, and a telemetry system to transmit all desired pressure, temperature, IMU, and flight computer data to ground receiving stations. All vehicle subsystems are illustrated in a preliminary internal arrangement in figure below

American Institute of Aeronautics and Astronautics
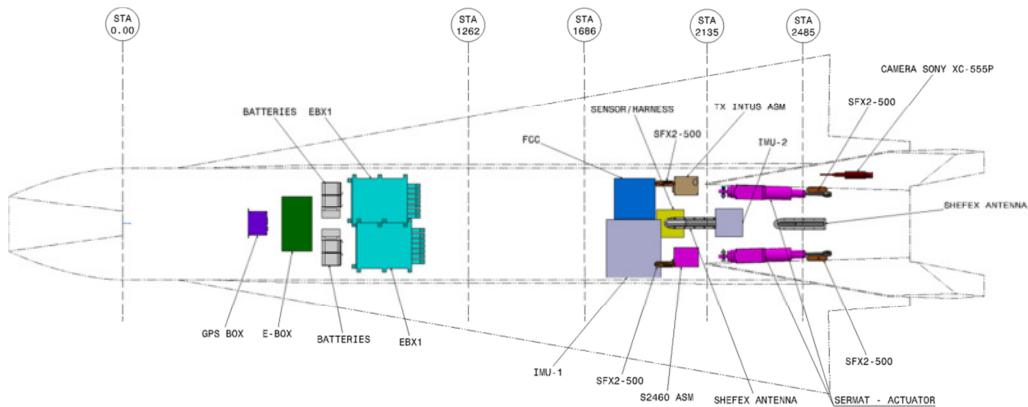
The Avionic System will perform the Vehicle Management through the following high level functions:

- ✓ To provide a HW platform for the implementation of the logics and the algorithms to guide and control the EFTV vehicle during the aerodynamic controlled phase;
- ✓ To provide an Electric Power source and to distribute the Power to all the subsystems throughout all the mission phases;
- ✓ To Acquire and Record on-board all the sensors data, functional to the mission control and of the
- ✓ scientific payloads;
- ✓ To Communicate by means of a bidirectional RF link with the Ground Control Station for Telemetry/Telecommands transmission

The control of the HEXI vehicle is performed through the aerodynamic surfaces while the EFTV+ESM train is controlled by means of a cold gas system (CGS) as dynamic pressure does not allow the control through aerodynamic surfaces in the portion of trajectory starting from the payload separation at apogee (i.e. 90 km) to the beginning of EFTV flight (separation of EFTV from ESM). The RCS is based on three groups of thrusters located in the ESM Module.

## V. Flight Mechanics

The reference mission scenario currently foreseen for the EFTV+ESM, and EFTV design is summarized from Figure 28 to Figure 30. The HEXAFLY-INT mission is conceived to achieve a hypersonic leveled flight at an altitude of about 30 km, while being injected from a semi-ballistic trajectory depicted in Figure 2, and described in Table 1.

After a boost provided by an expendable launch vehicle equipped by a solid rocket motor (S43), bringing the scientific payload (EFTV+ESM) to about 90 km apogee, it follows a ballistic phase in the high atmosphere stabilized by an attitude control system, through CGS, in combination with an aerodynamic flare (ESM).

The vehicle (EFTV) is detached from the ESM when ESM-EFTV separation conditions are reached (see next section for further details) . After the separation, a pull-out manoeuver brings EFTV to a hypersonic leveled flight at a target altitude of about 30 km. The FTV trajectory after ESM-EFTV separation is referred as trajectory B viscous.

American Institute of Aeronautics and Astronautics
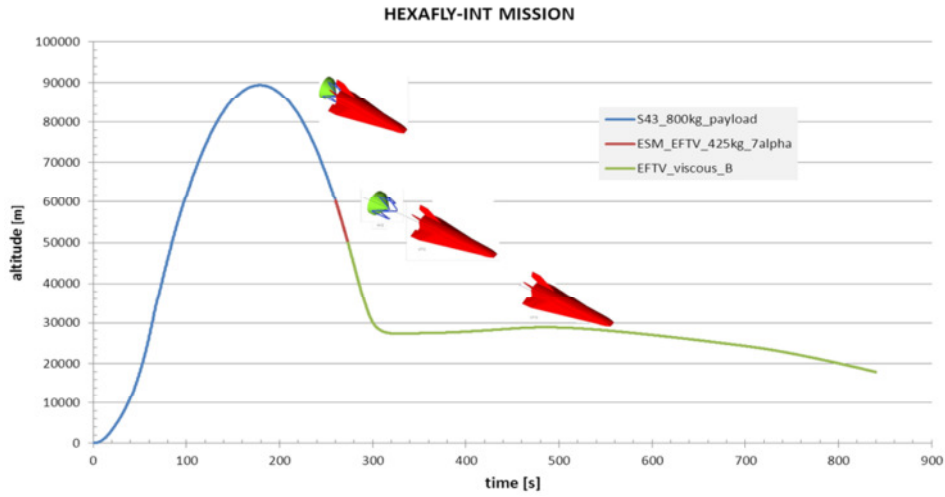
**Figure 28: Overall altitude time history.**

The Mach number time history is shown in Figure 29; while the overall time histories of AoA and aileron trim deflections are provided in Figure 30.
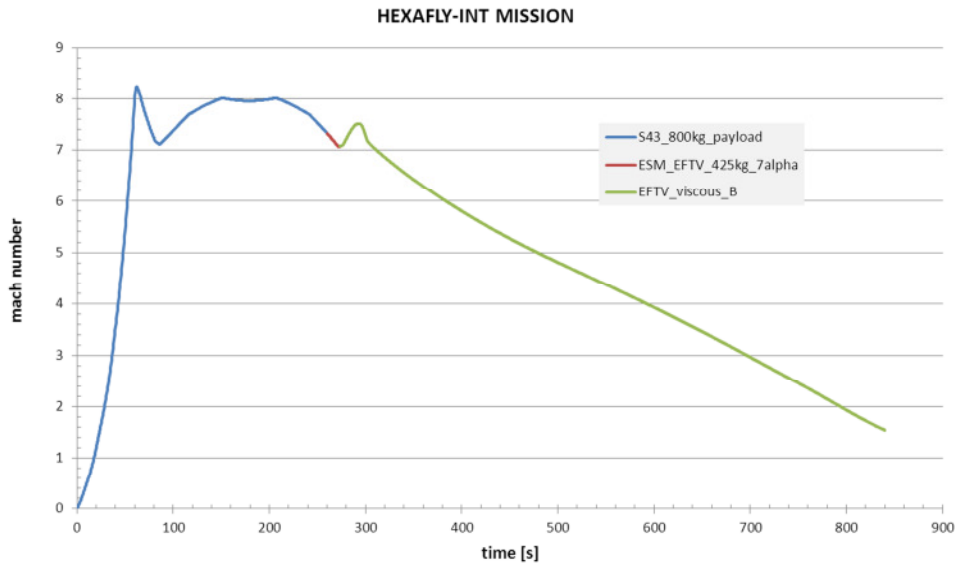


**Figure 29: Overall Mach number time history.**

American Institute of Aeronautics and Astronautics
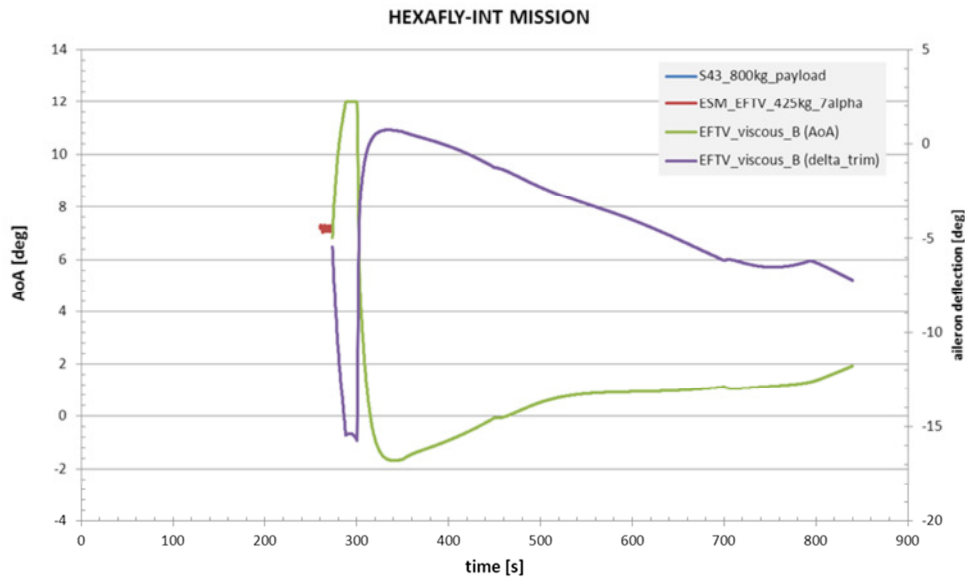
**Figure 30: Overall time histories of AoA and aileron trim deflection.**

Note that the trajectories have been generated by DLR-Moraba for what concerns the launch vehicle, assuming a total payload weight of 800 kg (EFTV, ESM, launch vehicle service module, fairing) for the S43 booster, and by Gas Dynamics Ltd. (GDL, partner of HEXAFLY-INT project) for both the EFTV+ESM train (i.e. from 60 km to the separation altitude), and for the EFTV after the separation from ESM down to 20 km of altitude.

*Separation Analysis*

During the HEXAFLY-INT experiment, before the separation of EFTV from ESM, the attitude control is in charge of CGS of service module After the separation, this task shall be accomplished by the Flight Control system on EFTV; for this reason, the separation between ESM and EFTV must occur at a flight condition such that the control system has enough authority to control the vehicle attitude. Therefore a specific flight condition has to be fixed from which the responsibility to control the EFTV is transferred from the CGS of ESM to the Flight Control System of EFTV.
The identification of a possible separation point is of paramount importance as this point shall be carefully selected in order to ensure that control authority can be reliably transferred from ESM to EFTV. This condition clearly depends on the dynamic pressure but also on the aerodynamic characteristics of the EFTV. The analysis has been based on the preliminary EFTV configuration data, i.e. longitudinal aerodatabase and the preliminary ESM-EFTV trajectory. As a result, the analysis will be repeated as far as both vehicle configuration and reference trajectory will be refined. Furthermore the analysis does not take into account parametric uncertainties.

In order to preliminary identify the possible separation point, a number of criteria have been defined starting from specialized literature and past projects in which the same problem has been faced (see refs. [10]-[12]). The defined criteria are based on the computation of some parameters depending on both the vehicle aerodynamic characteristics and the reference trajectory.

The analysis results show that the defined criteria can be satisfied provided that the separation between ESM and EFTV occurs at a dynamic pressure not lower than about 3000 Pa. According to the preliminary ESM-EFTV trajectory, this flight condition occurs at an altitude of about 50 km, a Mach number of about 7 and an angle of attack of 7 degrees..
Obviously a more conservative condition for the ESM-EFTV separation should be considered as the carried out analysis does not account for the uncertainties affecting the parameter involved in the evaluation of control authority.

American Institute of Aeronautics and Astronautics

Moreover, a further analysis has been carried out with the aim of finding the AoA range in which the criteria defined in this document can be satisfied. This may represent a useful indication for the selection of EFTV reference trajectory.

As it can be seen from the figure below, when dynamic pressure is lower than about 2020 Pascal it is not possible to find an admissible AoA range as maximum AoA is lower than minimum AoA. When dynamic pressure becomes higher, the criteria are satisfied provided that AoA is constrained to lie within an interval which becomes higher and higher as the dynamic pressure (and consequently the control authority) increases.
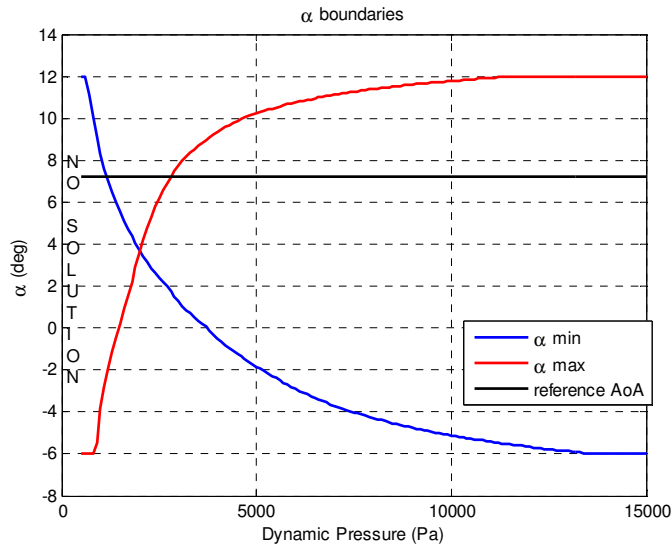


**Figure 31: AOA range satisfying all the criteria**

## VI. Concluding Remarks

The present paper has dealt with the design analysis of the experimental flight test vehicle under development in the seventh framework programme, namely HEXAFLY-INT.

A Waverider body shape unmanned re-entry vehicle has been studied as technological prototype in order to demonstrate the application of state of the art technologies of the different sub-systems.

The logical steps of the early phase of HEXI project are introduced. The choice and evolution of the aero shape has been described by means of analytical approach based on theoretical, semi-empirical and numerical basis. Once aerodynamics, flight mechanics and aerothermodynamics verify the capability of the aero shape to perform the mission, the system configuration development starts and, after some loops to fulfill the mission and system requirements, the baseline system configuration has been selected. In detail, a mission scenario, the different flight segments and events to which the payload is exposed to have been described and justified. This has allowed for the definition of the aero-thermo-mechanical loads required to conceptually design all elements on board of the vehicle. This flying test bed is a self-controlled glider configuration that shall face a levelled hypersonic flight at about Mach 8, just after the separation from the experimental support module at about 50 km altitude, up to the vehicle loss. During this flight several experiments shall be carried out. The appraisal of the vehicle aerodynamic performance is needed for Flight Mechanics and Guidance, Navigation and Control analysis.

It has to be highlighted that, at the time being, the HEXAFLY-INT project is closing the Preliminary Design Review and is fully focused on the detailed design of the systems and subsystems, for the launch vehicle, the EFTV and the ESM, while the related technology assessments are on-going. The Critical Design Review is foreseen in 2016.

## Acknowledgments

## References

[1] Steelant, J., Varvill R., Defoort S., Hannemann K. and Marini M., "*Achievements Obtained for Sustained Hypersonic Flight within the LAPCAT-II project.*" 20th AIAA International Space Planes and Hypersonic Systems and Technologies Conference, July Glasgow, Scotland. 2015.

[2] Steelant J., *"ATLLAS: Aero-Thermal Loaded Material Investigations for High-Speed Vehicles"*, 15th AIAA International Space Planes and Hypersonic Systems and Technologies Conference, 28/04-01/05-2008, Dayton, Ohio, USA, AIAA-2008-2582.

[3] Steelant J., "*European Activities on High-Speed Vehicles: Feasibility Studies and Technological Challenges for Hypersonic Cruisers*", Aerothermodynamics Conference ATD7, ATD7-215019, May 2011, Bruges, Belgium.

[4] Steelant J. et al., "*Conceptual Design of the High-Speed Propelled Experimental Flight Test Vehicle HEXAFLY*", 20th AIAA International Space Planes and Hypersonic Systems and Technologies Conference, July, Glasgow, Scotland. 2015.

[5] Weast, R.C. (1999). CRC Handbook of Chemistry and Physics, CRC Press, Boca Raton, FL, 80th Edition

[6] Glass, D.E., Capriotti, D.P., Reimer, T., Kütemeyer, M., Smart, M., "*Testing of DLR C/C-SiC and C/C for HIFiRE 8 Scramjet Combustor*", 19th AIAA "International Space Planes and Hypersonic Systems and Technologies Conference", 16-20 Jun. 2014 Atlanta, Georgia.

[7] Pezzella,G., Marini, M., Reimann, B., Steelant, J., "*Aerodynamic Design Analysis of the HEXAFLY-INT Hypersonic Glider*", 20th AIAA International Space Planes and Hypersonic Systems and Technologies Conference, July Glasgow, Scotland. 2015.

[8] Pezzella G., Carandente V., Scigliano R., Marini M., Steelant J., "*Aerothermal Environment Methodology Of The Hexafly-Int Experimental Flight Test Vehicle (EFTV)*", 8th European Symposium on Aerothermodynamics for Space Vehicles, 2-6 March 2015, Lisbon, Portugal.

[9] Carandente V., Scigliano R., Pezzella G., Marini M. and Steelant J., "*Finite Element thermal design of the Hexafly- INT Experimental Flight Test Vehicle*", 6th European Conference for Aeronautics and Space Sciences (EUCASS), 29 june – 03 july 2015, Krakow, Poland.

[10] MIL-STD-1797

[11] AGARD-R-577-70 "V/STOL Handling I-Criteria and Discussion" - 1970

[12] Alony A., Wahnon E., Attar M.; "DFCS SCA Flying Qualities Requirements for Control Laws Design", Israel Aircraft Industries LTD - Israel 2001